

THE ABUNDANCE OF FLUORINE IN NORMAL G AND K STARS OF THE GALACTIC THIN DISK

C. A. Pilachowski¹ & Cameron Pace¹

Astronomy Department, Indiana University Bloomington, Swain West 319, 727 East Third Street, Bloomington, IN 47405-7105, USA; cpilacho@indiana.edu, cjp@indiana.edu

ABSTRACT

The abundance of fluorine is determined from the (2-0) R9 2.3358 μm feature of the molecule HF for several dozen normal G and K stars in the Galactic thin disk from spectra obtained with the Phoenix IR spectrometer on the 2.1-m telescope at Kitt Peak. The abundances are analyzed in the context of Galactic chemical evolution to explore the contributions of supernovae and asymptotic giant branch (AGB) stars to the abundance of fluorine in the thin disk. The average abundance of fluorine in the thin disk is found to be $[\text{F}/\text{Fe}] = +0.23 \pm 0.03$, and the $[\text{F}/\text{Fe}]$ ratio is flat or declines slowly with metallicity in the range from $-0.6 < [\text{Fe}/\text{H}] < +0.3$, within the limits of our estimated uncertainty. The measured abundance of fluorine and lack of variation with metallicity in Galactic thin disk stars suggest neutrino spallation in Type II supernovae contributes significantly to the Galactic fluorine abundance, although contributions from AGB stars may also be important.

Subject headings: stars: abundances; stars: late type; Galaxy: abundances; Galaxy: disk

Facility: KPNO: 2.1m (Phoenix)

¹Visiting Astronomer, Kitt Peak National Observatory. KPNO is operated by AURA, Inc. under contract to the National Science Foundation.

1. Introduction

The abundances of a variety of chemical elements contribute to our understanding of the chemical evolution of the Milky Way Galaxy, including Li and CNO (Spite et al., 2005), the alpha-process elements and transition peak metals (Tinsley 1980), and the n-capture species (Snedden et al. 2003). The origin of the abundant, even-Z, light elements through Ca (and perhaps Ti) are reasonably well-understood through helium, carbon, neon, and oxygen burning, the silicon quasi-equilibrium process, and subsequent explosive nucleosynthesis in Type II supernovae (SNe II; Nomoto et al. 2013). The origin of the less abundant, odd-Z elements Na through Cl, particularly fluorine, phosphorus, and chlorine, is less well understood, yet these elements provide an opportunity to constrain secondary nucleosynthesis processes operating on more abundant species in SNe II supernovae. The odd-Z element abundances can also be modified through proton-capture reactions in low- and intermediate-mass asymptotic giant branch (AGB) stars (see, e.g. Cristallo et al. 2009; Ventura & D’Antona 2008), as seen, for example, in the unusual chemical evolution processes operating in globular clusters (e.g. Ventura et al. 2001; Gratton et al. 2012).

Briefly, the light, odd-Z element fluorine can be produced in a variety of astrophysical environments; for a full discussion of sources of fluorine, see recent papers by Kobayashi et al. (2011), Recio-Blanco et al. (2012), and Jönsson et al. (2014a). Potential sources in the Galaxy include SNe II, AGB stars, and possibly Wolf-Rayet stars (production of fluorine in Type Ia supernovae is thought to be small). Production in SNe II, however, is not sufficient to account for the abundance of fluorine in the Galaxy without the additional production due to the ν -process involving inelastic scattering of μ and τ neutrinos off ^{20}Ne (Woosley et al. 1990, Woosley et al. 2002, Kobayashi et al. 2011).

In AGB stars, fluorine is produced in core and shell helium-burning, but is destroyed by proton capture at the base of the convective envelope for stars with initial masses of 4-7 solar masses, and by alpha captures at temperatures above 2.5×10^8 K (see Lugaro et al. 2004 & 2012, Karakas et al. 2008, and Gallino et al. 2010). Thus, significant amounts of fluorine can be contributed only by AGB stars in the mass range 2-4 solar masses, so that fluorine from AGB stars should only be found in stars with metallicities greater than $[\text{Fe}/\text{H}] = -1.5$ (Kobayashi et al. 2011). We note, however, that more massive AGB stars (see e.g. García-Hernández et al. 2006, 2007) could overproduce fluorine to a smaller extent once hot bottom burning ceases (Karakas et al. 2010, Lugaro et al. 2012, D’Orazi et al. 2013). The enrichment of fluorine is less in more massive AGB stars but they expel much more material to the interstellar medium than do lower mass AGB stars.

Fluorine abundances in AGB stars have been reported in numerous studies, beginning with Jorissen et al. (1992), which has since been partly revised to lower values by Abia et al.

(2009, 2010). More recently, fluorine has been found in stars contaminated with products of AGB nucleosynthesis via mass transfer. Schuler et al. (2007) and Lucatello et al. (2011), for example, found enhanced fluorine in some carbon-enhanced metal-poor (CEMP) stars, which they attribute to contamination by former AGB companions. In addition, some authors have reported high fluorine abundances in second generation stars in globular clusters (see, for example, de Laverny & Recio-Blanco 2013, D’Orazi et al. 2013, and model predictions by Ventura & D’Antona, 2008). However, Kobayashi et al. (2011) concluded that AGB production of fluorine is not sufficient to account for the observed abundance of fluorine at the solar metallicity. Also of interest is the observation of fluorine enhancements in R Coronae Borealis and extreme helium stars (Pandey 2006, Pandey et al. 2008, and Jeffery et al. 2011).

Production in Wolf-Rayet (WR) stars during the early He-burning phase is also possible (e.g. Meynet & Arnould 1993, 2000), but the fluorine must be returned to the interstellar medium through stellar winds before temperatures in the He-burning zone exceed 2.5×10^8 K where fluorine is destroyed. Palacios et al. (2005) reexamined the production of fluorine by WR stars using newer yields and models including rotation, but noted that major uncertainties in yields remain. Jönsson et al. (2014a) suggested that contributions from WR stars may be required to account for trends in both $[F/Fe]$ and $[O/Fe]$ in Galactic bulge giants.

Observations of the Galactic abundance of fluorine require the determination of the fluorine abundance in less-evolved field stars not contaminated by AGB nucleosynthesis. Jorissen et al. (1992) included a handful of normal giants, and their sample was expanded by Cunha & Smith (2005) and by Recio-Blanco et al. (2012). More recently, Jönsson et al. (2014b) published analyses of the fluorine abundance in six nearby, cool giants (plus the thick disk giant Arcturus). In this paper, we report the abundance of fluorine in several dozen field giants and dwarfs residing in the Galactic thin disk, in order to determine the Galactic abundance of fluorine as a function of metallicity and to constrain the nucleosynthetic sources of fluorine contributing to chemical enrichment in the Milky Way. In Section 2, we describe the selection of targets, observational material, and analysis, and compare our results to the literature. In Section 3, we discuss our results in the context of the Galactic thin disk and chemical evolution models, and finally, in Section 4, we summarize our conclusions.

2. Observations and Analysis

2.1. Target Selection

Two criteria were used to select stars to be included in this study. First, stars must have available atmospheric parameters, including temperature, surface gravity, and $[\text{Fe}/\text{H}]$ from the literature, specifically from the Pastel Catalogue of Stellar Parameters (Soubiran et al. 2010). Atmospheric parameters are needed because the limited spectral region available with our Phoenix observations is not sufficient to determine spectroscopic parameters independently. Second, stars must be probable members of the Galactic thin disk.

The probability of stars to belong to the thin disk was estimated following the methodology of Johnson & Soderblom (1987), as described by Ramírez et al. (2013). For most stars, the U, V, and W space velocities were obtained from Casagrande et al. (2011); for stars not included in this catalog, we used available proper motion, parallax, and radial velocity data from SIMBAD to calculate the space motions, using the online tool provided by David Rodríguez¹. From the U, V, and W space velocities, the probability of membership in the thin disk, thick disk, and halo populations can be calculated; stars with probabilities of belonging to the thin disk of greater than 50% were then included in our analysis. Most stars in our sample have probabilities greater than 90% of belonging to the thin disk population, although six stars have membership probabilities in the range $0.75 < P < 0.9$ (HD 5268, HD 17660, HD 32147, HD 37984, HD 218031, and HD 222107) and two stars have less certain membership (HD 43039 at $P=0.56$ and HD 39715 at $P=0.67$).

2.2. Observations

Spectra of the $2.336 \mu\text{m}$ micron region containing a reasonably unblended feature of the molecule HF were obtained with the Phoenix spectrometer (Hinkle et al. 1998) on the 2.1-m telescope of the Kitt Peak National Observatory in 2012 November and December. This spectral region is dominated by strong lines of CO, with relatively few atomic lines. The spectrograph was configured with a 4-pixel ($107 \mu\text{m}$) slit corresponding to 0.7 arcsec on the sky. With the 4308 filter to isolate grating order 32, we obtained a spectral resolving power of 25,000 and spectral coverage from $2.3285\text{--}2.3390 \mu\text{m}$. Observations were obtained in pairs at two slit positions to facilitate dark current and sky subtraction. Typically four observations were obtained for each star at two different slit positions to remove thermal

¹<http://www.das.uchile.cl/~drodrigu/UVWCalc.html>; August 2013

emission from the sky. To minimize telluric absorption, stars were observed close to the meridian, with zenith distances typically less than 25 degrees (airmass < 1.1). Telluric lines were removed using the IRAF² task telluric, which shifts and scales the telluric line spectrum to minimize residual effects of telluric lines. Telluric line division was specifically optimized for the spectral region near the HF feature. Each star’s radial velocity shifts its HF feature relative to the telluric spectrum, so that each star is affected differently.

2.3. Analysis

The abundance of fluorine was determined using both spectrum synthesis and equivalent width analysis of the $2.3358\ \mu\text{m}$ feature. The equivalent width method provides a more robust upper limit in cases where the HF feature is not detected, or detection is questionable. The analysis utilized the LTE spectrum synthesis code Moog (Snedden 1973, 2010 version) and model atmospheres interpolated in the MARCS³ grid (Gustafsson et al. 2008).

Following D’Orazi et al. (2013), an excitation potential of $\chi=0.227\ \text{eV}$ was adopted for the $2.3358\ \mu\text{m}$ feature of HF from the HITRAN molecular line database (Rothman et al. 2013). As discussed by Nault & Pilachowski (2013), this value differs from the value of $0.49\ \text{eV}$ previously used in the literature (including in the original solar abundance determination by Hall & Noyes 1969), and results in a lower abundance of fluorine by typically $0.36\ \text{dex}^4$. The oscillator strength $\log gf = -3.971$ was adopted from Lucatello et al. (2011); this value is close to the value typically used in the literature (see, for example, Jorissen et al. 1992 and Recio-Blanco et al. 2012). The dissociation energy used by Moog is $5.8698\ \text{eV}$. Jönsson et al. (2014a) carefully examined the calculation of the partition functions for HF, and Jönsson et al (2014b) concluded that the partition functions used with Moog are in agreement with their calculations.

For spectrum synthesis of the neighboring CO (2–0) and (3–1) vibration-rotation lines, we adopted wavelengths, excitation potentials, and gf-values from Goorvitch (1994). A handful of atomic lines are present in the spectrum, and we adopted line parameters from

²IRAF is distributed by the National Optical Astronomy Observatory, which are operated by the Association of Universities for Research in Astronomy, Inc., under cooperative agreement with the National Science Foundation.

³The interpolation of models utilized code provided by Masseron (2006, <http://marcs.astro.uu.se/software.php>).

⁴We use the standard spectroscopic notation where $[A/B] \equiv \log(N_A/N_B)_{\text{star}} - \log(N_A/N_B)_{\odot}$ and $\log \epsilon(A) \equiv \log(N_A/N_H) + 12.0$ for elements A and B.

the Vienna Atomic Line Database (VALD) (Kupka et al 2000, and references therein) for our spectrum synthesis.

Since our spectral region is limited, with few atomic lines, we were unable to derive reliable stellar model atmosphere parameters from our spectra. Instead, we adopted temperatures, surface gravities ($\log g$), values of the microturbulence parameter (ξ), and metallicities from the literature, selecting sources wherever possible from large compendia. The adopted atmospheric parameters are included in Table 2 for all stars in our sample. The most frequently used sources for atmospheric parameters are the large samples studied by McWilliam (1990) and Prugniel et al. (2011), although several additional sources were needed to identify parameters for all stars in our sample. All sources are listed in the references for Table 2.

A synthetic spectrum of the HF region was computed for each star using the adopted model atmosphere parameters. Initial abundances for CNO were estimated based on the stellar metallicity and spectral type, and then adjusted to match the observed CO line strengths. Since the abundances of neither C nor O are available in the literature for most of our program stars, we are unable to determine abundances of these species from the CO lines alone. Once the CO spectrum was fit, the abundance of fluorine was adjusted to match the observed HF line profile. Sample observed and synthetic spectra are shown in Fig. 1.

The nearby (2-0) R25 line of $C^{12}O^{17}$ is present in some spectra, and was included in the synthesis calculation to account for possible blending with the HF feature. The O^{16}/O^{17} ratio varies from a few hundred in giant stars to a few thousand in dwarf stars (Clayton 2003), and the presence of possible contamination from $C^{12}O^{17}$ can be estimated from other stronger, unblended features in the observed spectral range.

Equivalent widths of the relatively isolated $2.3358 \mu m$ feature of HF were also measured from the observed spectra using the *splot* task in IRAF with a Gaussian fit to the line. If present, the $C^{12}O^{17}$ feature was also fit with a Gaussian to eliminate its contribution to the HF equivalent width.

The *abfind* driver from Moog was used to obtain the abundances of fluorine from the measured equivalent widths using the same model atmosphere as for the syntheses. Values of the equivalent width of HF range from lower limits of $<10 \text{ m}\text{\AA}$ to $250 \text{ m}\text{\AA}$ ($\log W/\lambda = -4.97$). The measured equivalent widths or equivalent width upper limits are included in Table 2.

The two methods of analysis provide similar results for fluorine, typically within 0.2 dex in $\log \epsilon(F)$, with an average difference of 0.09 dex. Sources of uncertainty from the spectrum synthesis include both the continuum level and the smoothing factor to match the instrumental profile. Uncertainties in equivalent widths are dominated by the continuum height, as well as noise for cases with weak HF lines or lower S/N ratio. Both methods are affected

similarly by uncertainties in the atmospheric parameters and atmospheric modeling. The two results were averaged in most cases. When the two results were discrepant, an overly optimistic fit of the synthetic spectrum to noise was generally the cause; in these cases, the equivalent width provides a more realistic upper limit.

The final adopted values of the abundance of fluorine are included in Table 2, and are plotted versus effective temperature in Fig. 2. The abundance of fluorine is flat across a range of stellar temperatures, except at the warm end above 4600 K, where the HF feature becomes too weak and most measurements are upper limits unless the fluorine abundance is high. The HF feature disappears in stars hotter than about 4700 K due to molecular dissociation, so our effective sample is limited to stars with temperature below this limit. Our sample may contain an incompleteness bias for stars with $4500 \text{ K} < T_{\text{eff}} < 4700$, since detection of HF depends on both the S/N ratio of the spectrum and the metallicity of the star. The upper limit for HD 220009 at $T_{\text{eff}} = 4314 \text{ K}$ results from the low metallicity of the star at $[\text{Fe}/\text{H}] = -0.7$. The apparent rise in $\log \epsilon(\text{F})$ with temperature is likely due to observational limitations rather than a systematic temperature error.

The M0Iab supergiant HD 216946 (HR 8726) is labelled in Fig. 2. The star exhibits an anomalously high fluorine abundance, and may be affected by in situ proton capture nucleosynthesis. The star will not be considered further here.

Li et al. (2013) have considered deviations from radiative equilibrium in the formation of the HF R9 line, specifically due to 3D effects in the stellar atmospheres. The investigations of Li et al. apply in the low metallicity regime near $[\text{M}/\text{H}] = -2.0$. They found that 3D abundance corrections for HF are small (< 0.03 dex) at low gravity and temperature but increase with gravity and temperature to values near 0.42 dex at 5024 K and $\log g = 2.5$. Asplund (2005) notes that the corrections to apply to 1D models are more significant at lower metallicity, although such effects are generally more significant for molecular features than for atomic features. The stars considered here are all near-Solar in abundance, so corrections should be less for these stars than for metallicities near $[\text{Fe}/\text{H}] = -2$, and the absence of a dependence of derived abundance on temperature in Figure 2 gives some confidence that 3D effects do not increase significantly with temperature for stars below 4500 K. Restricting our sample to stars with effective temperatures below 4500 K, we also note that the average fluorine abundance for thin disk giants is $[\text{F}/\text{Fe}] = +0.23 \pm 0.03$ (standard error of the mean (SEM)), while the average abundance in the dwarfs is $[\text{F}/\text{Fe}] = +0.19 \pm 0.12$ (SEM), likely the same within our estimated uncertainties.

Observational uncertainties in the fluorine abundance can be estimated from discernable differences in the synthetic spectrum fits (± 0.05 dex). Additional uncertainties, both random and systematic, arise from the selection of atmospheric parameters. Among the various

atmospheric parameters, the abundance of fluorine is most sensitive to errors in effective temperature due to the relatively low dissociation potential of HF. Since we relied on multiple sources for atmospheric parameters, we have no guarantee of consistency of the temperature scale, particularly over the range of spectral type (G5 to M0) and luminosity class (V to Iab) represented in our sample. In principle, we might expect star-to-star errors in temperature of perhaps 30 K for stars from particular literature sources, and 100 K in the full sample. A temperature error of 100 K would lead to an error of ~ 0.25 dex; errors introduced from uncertainties in surface gravity, microturbulence, and metallicity are all small, less than 0.1 dex, as shown in Table 3. Combining errors in quadrature suggests an uncertainty of 0.26 dex. On the other hand, at a given metallicity, the dispersion in the measured fluorine abundances is ~ 0.24 dex. The observed scatter in $\log \epsilon(\text{F})$ is consistent with a measurement uncertainty of 0.26 dex.

2.4. Comparison to Previous Work

Our fluorine abundances for thin disk stars are compared in Figure 3 (upper panel) to other works that have included normal, thin disk dwarfs and giants not exhibiting other evidence of contamination from AGB nucleosynthesis. Nearby dwarf stars are available from Recio-Blanco et al. (2012), field giants were included by Jorissen et al. (1992), Cunha & Smith (2005), and Jönsson et al. 2014b; and open cluster giants have been reported by Nault & Pilachowski (2013) and Maiorca et al (2014). Fluorine abundances from Recio-Blanco et al., Jorissen et al., and Cunha & Smith all used the older excitation potential for the HF feature, consistent with the original solar abundance of fluorine reported by Hall and Noyes (1969), and $[\text{F}/\text{Fe}]$ values are computed relative to a solar abundance of $\log \epsilon = 4.56$. Jönsson et al. used similar molecular data to ours and their $[\text{F}/\text{Fe}]$ ratios are calculated using the new Maiorca et al. (2014) solar abundance.

Compared to other studies of the abundance of fluorine in thin disk stars in the solar neighborhood, our much larger sample covers a wider range of metallicity in the thin disk ($-0.6 < [\text{Fe}/\text{H}] < +0.3$) and includes stars in the restricted temperature range $3800 < T_{\text{eff}} < 4500$ K in which the HF feature is strong enough to be easily measured. Adopting the new Maiorca et al. (2014) solar fluorine abundance of $\log \epsilon(\text{F}) = 4.40$ (Maiorca et al. used the same molecular data as are used in this paper), the average fluorine abundance of our sample of nearly 40 stars with $T_{\text{eff}} < 4500$ K is $[\text{F}/\text{Fe}] = +0.23 \pm 0.03$ (SEM). This result compares with an average abundance $[\text{F}/\text{Fe}] = +0.24 \pm 0.06$ (SEM) for the Recio-Blanco et al. (2012) sample of nine dwarf stars and an average of $[\text{F}/\text{Fe}] = +0.21 \pm 0.03$ (SEM) for the seven normal thin disk giants included by Jorissen et al. (1992). In contrast,

Jönsson et al. (2014b) find $[F/Fe] = -0.04 \pm 0.05$ (SEM) from their analysis of the $12\ \mu\text{m}$ HF feature in six cool K and M giants.

Each of these studies has adopted different approaches for determining the model atmosphere parameters. Some rely on parameters determined from optical spectra (Recio-Blanco et al. 2012 and this paper), one relies on a temperature vs. spectral type relation (Jorissen et al. 1992 from Smith & Lambert 1990), one relies on broadband colors (Cunha & Smith 2005) and one relies on optical angular diameter measurements (Jönsson et al. 2014b). Given the sensitivity of the derived fluorine abundance to temperature (typically 0.25 dex per 100 K temperature change; see Table 3), temperature scale errors likely dominate the uncertainty in the average fluorine abundance of the local thin disk. The average fluorine abundance in the solar neighborhood remains uncertain at the level of 0.2 dex.

A formal fit to the dependence of $[F/Fe]$ on $[Fe/H]$ for our sample of stars with well-determined abundances gives $[F/Fe] = -0.105[Fe/H] + 0.20$, suggesting an average fluorine abundance of $[F/Fe] = +0.20$ ($\log \epsilon(F) = 4.6$) at the solar metallicity, somewhat higher than the Lodders et al. (2009) meteoritic abundance of $\log \epsilon(F) = 4.42$ or the new Maiorca et al. (2014) solar photospheric abundance of $\log \epsilon(F) = 4.40$. The Sun may be slightly deficient in fluorine compared to the solar neighborhood, but a firm conclusion awaits a self-consistent determination of stellar atmospheric parameters using infrared spectra.

3. Fluorine Enrichment in the Thin Disk

Given the variety of possible sources of fluorine in the Milky Way (SNe II, AGB stars, WR stars, etc.), observations of fluorine in uncontaminated field stars may provide clues about the principal contributor of the element to the Galactic disk today. Of particular interest is the relationship between fluorine and other light elements that are affected by proton-capture nucleosynthesis. Studies of fluorine and oxygen in AGB stars exhibiting the products of the third dredge-up find a correlation between $[F/Fe]$ and $[O/Fe]$ (see, for example, the fluorine abundances from Abia et al. 2010 and the oxygen abundances from Lambert et al. 1986 for the same stars, as well as the Cunha et al. 2003 samples from the Milky Way and Large Magellanic Cloud).

The average fluorine in N-type carbon stars by Abia et al. (2010) is $[F/Fe] = 0.27 \pm 0.04$ (SEM). Abia et al. note the relatively low fluorine abundances of the N-type stars compared to SC-type AGB stars, as well as the similarity of their fluorine abundances to those of K and M field stars at evolutionary phases prior to the AGB. These abundances are suggestive that at least some N-type carbon stars in the Milky Way are only modestly enhanced in

fluorine, if at all.

Observations of light elements in globular cluster stars (Carretta et al. 2009, Mészáros et al. 2015) have demonstrated a substantial spread in light element abundances attributed to proton-capture nucleosynthesis, most likely occurring in an earlier generation of metal-poor, intermediate-mass, hot-bottom-burning AGB stars (although fast-rotating massive stars may also play a role). Studies of fluorine in globular cluster giants (Cunha et al. 2003, Smith et al. 2005, Yong et al. 2008, D’Orazi et al. 2013, de Laverny & Recio-Blanco 2013) have shown both a correlation of fluorine and oxygen and an anti-correlation of fluorine and sodium, for clusters in the metallicity range $-1.2 \leq [\text{Fe}/\text{H}] \leq -0.7$. Observations of HF in cluster giants are, however, very difficult because of the low metallicity and relatively warm temperatures of even the coolest red giants. The HF feature is typically weak compared to residual features from telluric line correction (D’Orazi et al. 2013).

Fluorine production in AGB stars occurs primarily in 2-4 solar mass stars according to Nomoto et al. (2013), although more massive AGB stars may also produce excess fluorine once hot bottom burning (which destroys fluorine) ceases (see Karakas 2010, Lugaro et al. 2012, and D’Orazi et al. 2013 for a more complete discussion). If present in normal stars in the Galactic thin disk, a fluorine-oxygen correlation and fluorine-sodium anti-correlation in thin disk stars might indicate some substantial contribution of AGB stars to the fluorine abundance in the thin disk. The question is complicated, however, by the possibility of metallicity dependent yields from the various potential sources of fluorine in the Milky Way.

The existence of a fluorine-oxygen correlation is examined explicitly for the thin disk in Fig. 4. Oxygen abundances are available from the literature for only a few of the stars in the combined sample of new and previously published stars with fluorine abundances, and are plotted as $[\text{F}/\text{O}]$ vs. $[\text{O}/\text{H}]$ in the upper panel of Fig. 4. Models of the Galactic chemical evolution of fluorine and oxygen by Kobayashi et al. (2011) suggest that the $[\text{F}/\text{O}]$ ratio for fluorine production by AGB stars plus SNe (without neutrino spallation) should be relatively flat, with $[\text{F}/\text{O}] \approx -0.15$, while models that include neutrino spallation produce a higher $[\text{F}/\text{O}]$ ratio ($[\text{F}/\text{O}] = +0.2$), also with no dependence of $[\text{F}/\text{O}]$ on $[\text{O}/\text{H}]$. The average $[\text{F}/\text{O}]$ abundance for the sample of available data, including the low fluorine abundances from Jönsson et al. (2014b), is $[\text{F}/\text{O}] = +0.10 \pm 0.05$ (SEM), suggesting significant contributions from SNe II with neutrino spallation to the abundance of fluorine in the thin disk. The Kobayashi et al. models suggest that 2-4 solar mass AGB stars began to contribute substantially to the abundance of fluorine in the Galaxy at an oxygen abundance of $[\text{O}/\text{H}] = -1.2$, then reached a plateau at $[\text{O}/\text{H}] = -0.5$. From the $[\text{O}/\text{Fe}]$ versus $[\text{Fe}/\text{H}]$ data of Bensby et al. (2004), this oxygen abundance corresponds to $[\text{Fe}/\text{H}]$ of perhaps -0.9 dex.

In Fig. 5, the fluorine abundances $[\text{F}/\text{Fe}]$ are plotted vs. $[\text{Fe}/\text{H}]$, this time overlain

with the Kobayashi et al. (2011) predictions for three nucleosynthesis models: standard supernovae (including SNe II, hypernovae, and SNIa), supernovae plus contributions from AGB stars, and, finally, with additional contributions from the ν -process in core-collapse supernovae. The reader is cautioned, however, that the Kobayashi et al. models do not include possible contributions from WR stars. Since oxygen abundances are available for so few stars in our sample, $[\text{F}/\text{Fe}]$ and $[\text{Fe}/\text{H}]$ ratios have been obtained from the Kobayashi et al. models by assuming a linear correlation between the $[\text{O}/\text{Fe}]$ and $[\text{Fe}/\text{H}]$ ratios for thin disk stars in this metallicity range from Bensby et al. (2004), combined with the $[\text{O}/\text{H}]$ and $[\text{F}/\text{O}]$ model predictions.

We note first that, although the scatter in our measurements is large, the observed abundance of fluorine in the local thin disk matches well the predictions of Kobayashi et al. (2011) for models including neutrino spallation, and is well above the prediction for production dominated by AGB stars. The average abundance of fluorine at solar metallicity for our data is $[\text{F}/\text{Fe}] = +0.2 \pm 0.03$ (SEM), while the models predict $[\text{F}/\text{Fe}] = 0.18$ for the case of a neutrino explosion energy of 3×10^{53} erg, and higher for higher neutrino explosion energies.

The slope of the dependence of $[\text{F}/\text{Fe}]$ on $[\text{Fe}/\text{H}]$ is also consistent with the models including neutrino spallation within our estimated uncertainties. For our data in the range $-0.6 < [\text{Fe}/\text{H}] < +0.3$, we obtain a slope of -0.105 ± 0.14 per dex, compared to the model prediction of -0.18 per dex. In contrast, Kobayashi et al.’s (2011) model for fluorine production from AGB stars and SNe II without neutrino spallation indicates that the $[\text{F}/\text{Fe}]$ ratio should increase by 0.2 dex over the same metallicity range. Such an increase is inconsistent with our observations of a flat or slowly decreasing $[\text{F}/\text{Fe}]$ ratio with metallicity at the solar metallicity. Measurements of the slope of the $[\text{F}/\text{Fe}]$ vs $[\text{Fe}/\text{H}]$ dependence are independent of any systematic errors in temperature scale. The uncertainty on the measured slope can be reduced with better determinations of the atmospheric parameters, particularly the stellar effective temperatures.

Both the observed decrease of $[\text{F}/\text{Fe}]$ with $[\text{Fe}/\text{H}]$ and the average value of $[\text{F}/\text{Fe}]$ at the solar metallicity appear to support significant contributions of fluorine from supernovae through neutrino spallation in SNe II. Our conclusion is in contrast to the conclusions of both Recio-Blanco et al. (2012) and Jönsson et al. (2014b). Recio-Blanco et al. found, based in part on a possible correlation of $[\text{F}/\text{Fe}]$ with s-process abundances and the apparent absence of a correlation of $[\text{F}/\text{Fe}]$ with alpha elements, that AGB stars were the likely producers of fluorine in the Galactic disk. However, their analysis included only nine relatively warm main sequence stars ($T_{\text{eff}} > 4500$ K) with quite weak HF features, and their statistical correlations between fluorine and the s-process and alpha elements are low (≈ 0.5), as they note. Given

their small sample size and the amplitude of any trends compared with their uncertainties, the Recio-Blanco et al. sample does not provide compelling evidence for AGB-dominated production of fluorine.

Jönsson et al. (2014b), conclude that only AGB production of fluorine is needed to account for the abundance of fluorine in their sample of six cool, thin disk giants. Their conclusion is based on the relatively low derived abundance of fluorine in five of their six thin-disk giants, comparing to model predications of both $[F/Fe]$ and $[F/O]$. Given the temperature sensitivity of HF due to its low dissociation energy, combined with the extrapolation of interferometric diameters from optical wavelengths to determine temperatures in the infrared, systematic errors may affect their fluorine abundances at the level of 0.2 dex, which might alter their conclusions about its origin.

In the end, the source of fluorine in the Galactic thin disk remains relatively unconstrained by the observations, particularly given the diversity of potential sources of the element. Systematic errors among the temperature scales of the abundance determinations remain a significant source of uncertainty, as do the model predictions in light of the recent revision of the solar abundance of fluorine downward (Maiorca et al. 2014). The lack of oxygen abundance measurements in the same stars also limits our ability to constrain fluorine production models. Production in AGB stars remains a strong contender because of the observation of enhancements in fluorine in some AGB stars, but those enhancements, while interesting, are not themselves compelling evidence for a dominant role for AGB stars in Galactic chemical evolution. The question is further clouded by the discovery of strong fluorine enhancements in some CEMP stars (Schuler et al. 2007 and Lucatello et al 2011), and of strong fluorine enhancements in AGB stars in the metal-poor Large Magellanic Cloud (Abia et al. 2011), forcing metallicity-dependent yields into the mix of production scenarios.

4. Summary

Fluorine abundances have been determined for several dozen dwarf and giant stars identified as belonging to the Galactic thin disk to characterize the abundance of fluorine and its possible nucleosynthesis sources. We enumerate our basic conclusions below.

- Studies of normal stars in the Milky Way thin disk provide an opportunity to constrain models of fluorine nucleosynthesis. We provide the largest sample of normal stars yet analyzed for fluorine abundances.
- In the metallicity range $-0.6 \leq [Fe/H] \leq +0.3$, we find an average $[F/Fe]$ ratio of $+0.22 \pm 0.03$ (SEM), although systematic errors in the temperature scale may con-

tribute an uncertainty of 0.2 dex in comparing different studies.

- In the same metallicity range, the $[F/Fe]$ ratio is constant or slowly declining with metallicity, within our estimated uncertainties.
- The abundance of fluorine compared to oxygen in the thin disk is slightly high, typically $[F/O] = +0.10 \pm 0.05$.
- The observed $[F/Fe]$ abundance in the thin disk, the measured slope of the $[F/Fe]$ versus $[Fe/H]$ relation, and the relatively high $[F/O]$ ratio all provide evidence for contributions from the neutrino process in core-collapse supernovae to the abundance of fluorine in the thin disk and are inconsistent with fluorine production only in AGB stars.
- The presence or absence of correlations or anti-correlations of $[F/Fe]$ with $[O/Fe]$ or $[Na/Fe]$ may tell us about the contributions of AGB stars and/or fast-rotating massive stars toward the production of fluorine through proton-capture processing the Milky Way disk, but more accurate measurements of the $[F/Fe]$ ratio are needed, as are measurements of the oxygen abundance in the same stars.
- The origin of fluorine in the Galactic disk remains relatively unconstrained by observations, both because of possible systematic errors in temperature scale and because of insufficient data for other light elements in the same stars.

We are grateful to the Kitt Peak National Observatory and particularly to Dick Joyce and Krissy Reetz for their assistance at the start of the observing run. This research has made use of the NASA Astrophysics Data System Bibliographic Services, the HITRAN database operated by the Center for Astrophysics, and the WEBDA database and Vienna Atomic Line Database, both operated at the Institute for Astronomy of the University of Vienna. This research has made use of the SIMBAD database, operated at CDS, Strasbourg, France. We thank Eric Ost for implementing the model atmosphere interpolation code. Finally, we thank an anonymous referee for detailed comments on the manuscript. C.A.P. acknowledges the generosity of the Kirkwood Research Fund at Indiana University.

References

- Abia, C. Recio-Blanco, A., de Laverny, P., Chritallo, S., Domínguez, I., & Straniero, O. 2009, *ApJ*, 694, 971
- Abia, C., Cunha, K., Cristallo, S., de Laverny, P., Domínguez, I., Eriksson, K., Gialanella, L., Hinkle, K., Imbriani, G., Recio-Blanco, A., Smith, V. V., Straniero, O., & Wahlin, R. 2010, *ApJ*, 715, L94
- Abia, C., Cunha, K., Cristallo, S., De Laverny, P., Domínguez, I., Recio-Blanco, A., Smith, V. V., & Straniero, O. 2011, *ApJ*, 737, L8
- Allende Prieto, C., Barklem, P. S., Lambert, D. L., & Cunha, K. 2004, *A&A*, 420, 183
- Asplund, M. 2005, *ARAA*, 43, 481
- Balachandran, S. C., Fekel, F. C., Henry, G. W., & Uitenbroek, H. 2000, *ApJ*, 542, 978
- Bensby, T.; Feltzing, S.; & Lundström, I. 2004, *A&A*, 415, 155
- Carretta, E., Bragaglia, A., Gratton, R. G., Lucatello, S., Catanzaro, G., Leone, F., Bellazzini, M., Claudi, R., D’Orazi, V., Momany, Y., Ortonaly, S., Pancino, E., Piotto, G., Recio-Blanco, A., Sabbi, E. 2009, *A&A*, 505, 117
- Casagrande, L., Schönrich, R., Asplund, M., Cassisi, S., Ramírez, I., Meléndez, J., Bensby, T., & Feltzing, S. 2011, *A&A*, 530, 138
- Cristallo, S., Straniero, O., Gallino, R., Piersanti, L., Domínguez, I., & Lederer, M. T. 2009, *ApJ*, 696, 797
- Clayton, D. 2003, *Handbook of Isotopes in the Cosmos Hydrogen to Gallium* (Cambridge: Cambridge University Press)
- Cunha, K.; Smith, V. V.; Lambert, D. L.; Hinkle, K. H. 2003, *AJ*, 126, 1305
- Cunha, K., & Smith, V. V. 2005, *ApJ*, 626, 425
- de Laverny, P. & Recio-Blanco, A. 2013, *A&A*, 555, 121
- D’Orazi, V.; Lucatello, S.; Lugaro, M.; Gratton, R. G.; Angelou, G.; Bragaglia, A.; Carretta, E.; Alves-Brito, A.; Ivans, I. I.; Masseron, T.; & Mucciarelli, A. 2013, *ApJ*, 763, 22
- Gallino, R., Bisterzo, S., Cristallo, S., & Straniero, O. 2010, *Mem. Soc. stron. Ital.*, 81, 998
- García-Hernández, D. A., García-Lario, P, Plez, B., et al. 2006, *Science*, 314, 1751
- García-Hernández, D. A., García-Lario, P, Plez, B., et al. 2007, *A&A*, 462, 711

- Goorvitch, D. 1994, *ApJS*, 95, 535.
- Gratton, R. G., Carretta, E., & Bragaglia, A. 2012, *Astron. Astrophys. Rev.* 20, 50
- Gustafsson B., Edvardsson B., Eriksson K., Jorgensen U.G., & Nordlund, Å., & Plez B. 2008, *A&A*486, 951.
- Hall, D. N. B. & Noyes, R. W. 1969, *ApJ*, 4, 13
- Hekker, S., & Meléndez 2007, *A&A*, 475, 1003
- Hinkle, K.H., Cuberly, R., Gaughan, N., Heynssens, J., Joyce, R.R. Ridgway, S.T., Schmitt, P., and Simmons, J.E. 1998, *Proc. SPIE* 3354, 810
- Jeffery, S. C., Karakas, A. I., & Saio, H. 2011, *MNRAS*, 414, 3599
- Johnson, D. R. H., & Soderblom, D. R. 1987, *AJ*, 93, 864
- Jönsson, H., Ryde, N., Harper, G. M., Cunha, K., Schultheis, M., Eriksson, K., Kobayashi, C., Smith, V. V., & Zoccali, M. 2014a, *A&A*, 564, A122
- Jönsson, H., Ryde, N., Harper, G. M., Richter, M. J., & Hinkle, K. H. 2014b, *ApJ*, 789, L41
- Jorissen, A.; Smith, V. V.; & Lambert, D. L. 1992, *A&A*, 261, 164
- Karakas, A. I., Lee, H. Y., Lugaro, M., Görres, J. & Wiescher, M. 2008, *ApJ*, 676, 1254
- Karakas, A. I. 2010, *MNRAS*, 403, 1413
- Kobayashi, C., Izutani, N., Karakas, A. I., Yoshida, T., Yong, D., & Umeda, H. 2011, *ApJ*, 739, L57
- Kotoneva, E., Shi, J. R., & Zhao, G. 2006, *A&A*, 454, 833
- Kupka F., Ryabchikova T.A., Piskunov N.E., Stempels H.C., & Weiss W.W. 2000, *BaltA*, 9, 590
- Lambert, D. L., Gustafsson, B., Eriksson, K., & Hinkle K. H. 1986, *ApJ*, 62, 373
- Li, H. N., Ludwig, H.-G., Caffau, E., Christlieb, N. & Zhao, G. 2013, *ApJ*, 765, 51
- Lodders, K., Palme, H., & Gail, H.-P. 2009, *Landolt-Börnstein*, 44
- Lucatello, S.; Masseron, T.; Johnson, J. A.; Pignatari, M.; Herwig, F. 2011, *ApJ*, 729, 40
- Luck, R. E., & Bond, H.E. 1980, *AJ*, 241, 218
- Luck, R. E. & Heiter, U. 2006, *AJ*, 131, 3069

- Lugaro, M., Ugalde, C., Karakas, A. I., Görres, J., Weischer, M., Lattanzio, J., C., & Cannon, R. C. 2004, *ApJ*, 615, 934
- Lugaro, M., Karakas, A. I., Stancliffe, R. J., & Rijs, C. 2012, *ApJ*, 747:2
- Lyubimkov, L. S., Lambert, D. L., Rostopchin, S. I., Rachkovskaya, T., & Poklad, D. B. 2010, *MNRAS*, 402, 1369
- Maiorca, E., Uitenbroek, H., Uttenthaler, S., Randich, S., Musso, M., & Magrini, L. 2014, *ApJ*, 788, 149
- Masseron, T. 2006, PhD thesis, Obs. de Paris
- Mészáros, Sz., Martell, S. L., Shetrone, M. et L. 2015, *AJ*, 149, 153
- McWilliam, A. 1990, *ApJS*, 74, 1075
- Meléndez, J., Asplund, M., Alves-Brito, A., Cunha, K., Barbuy, B., Bessell, M. S., Chappini, C., Freeman, K. C., Ramírez, I., Smith, V. V., & Yong, D. 2008, *A&A*, 484, L21
- Meynet, G. & Arnould, M. 1993, in *Nuclei in the Cosmos II*, ed. Käppeler, F., Wisshak, E., (Bristol, IOP), p. 503
- Meynet, G. & Arnould, M. 2000, *A&A*, 355, 176
- Mishenina, T. V., Bienaymé, O., Gorbaneva, T. I., Charbonnel, C., Soubiran, C., Korotin, S. A., & Fovtyukh, V. V. 2006, *A&A*, 456, 1109
- Mishenina, T. V., Soubiran, C., Bienaymé, O., Korotin, S. A., Belik, S. I., Usenko, I. A., & Kovtyukh, V. V. 2008, *A&A*, 489, 923
- Nault, K. A. & Pilachowski, C. A. 2013, *AJ*, 146, 153
- Nomoto, K.; Kobayashi, C., & Tominaga, N. 2013, *ARA&A*, 51, 457
- Palacios, A., Arnould, M., & Meynet, G. 2005, *A&A*, 443, 243
- Pandey, G. 2006, *ApJ*, 648, L143
- Pandey, G., Lambert, D. L., & Rao, N. K. 2008, *ApJ*, 674, 1068
- Prugniel, Ph., Vauglin, I', & Koleva, M. 2011, *A&A*, 531, A165
- Ramírez, I. & Allende Prieto, C. 2011, *ApJ*, 743:135
- Ramírez, I., Allende Prieto, C., & Lambert, D. L. 2013, *ApJ*, 764:78

- Ramírez, S. V., Sellgren, K., Carr, J. S., Balachandran, S. C., Blum, R., Terndrup, D. M., & Steed, A. 2000, *ApJ*, 537, 205
- Recio-Blanco, A., de Laverny, P., Worley, C., Santos, N. C., Melo, C. & Israelian, G. 2012, *A&A*, 538, 117
- Rothman, L. S., Gordon I. E., Babikov, Y., et al. 2013, *JQSRT*, 130, 4
- Schuler, S. C., Cunha, K., Smith, V. V., Sirvarnai, T., Beers, T. C., & Lee, Y. S. 2007, *ApJ*, 667, 81
- Smith, V. V. & Lambert, D. 1990, *ApJS*, 72, 387
- Smith, V. V., Cunha, K., Ivans, I. I., Lattanzio, J. C., Campbell, S., & Hinkle, K. H. 2005, *ApJ*, 633, 392
- Snedden, C. 1973, *ApJ*, 184, 839
- Snedden, C., Cowan, J. J., Lawler, J. E., et al. 2003, *ApJ*, 591, 936
- Soubiran, C., Le Campion, J.-F., Cayrel de Strobel, G., & Caillo, A. 2010, *A&A*, 515, A111
- Sousa, S. G., Santos, N. C., Mayor, M., Udry, S., Casagrande, L., Israelian, G., Pepe, F. Wueloz, D. & Monteiro, M. J. P. F. G. 2008, *A&A*, 487, 373
- Spite, M., Cayrel, R., Plez, B., Hill, V., Spite, F., Depagne, E., Francios, P., Bonifacio, P., Barbuy, B., Beers, T., Andersen, J., Molaro, P., Nordström, B., & Primas, F. 2005, *A&A*, 430, 655
- Takeda, Y., Sato, B., & Murata, D. 2008, *PASJ*, 60, 781
- Tinsley, B. 1980, *FCPh*, 5, 287
- Valenti, J. A., & Fischer, D. A. 2005, *ApJS*, 159, 141
- Ventura, P. & D’Antona, F., Mazzitelli, I., & Gratton, R. 2008, *ApJ*, 550, L65
- Ventura, P. & D’Antona, F. 2001, *A&A*, 479, 805
- Wallace, L. & Livingston, W. 1992, N.S.O. Technical Report #92-001.
- Woosley, S. E.; Hartmann, D. H.; Hoffman, R. D.; & Haxton, W. C. 1990, *ApJ*, 356, 272
- Woosley, S. E., Heger, A., & Weaver, T. A. 2002, *Review of Modern Physics*, 74, 1015
- Yong, D., Meléndez, J., Cunha, K., Karakas, A. I., Norris, J. E., & Smith, V. V. 2008, *ApJ*, 689, 1020

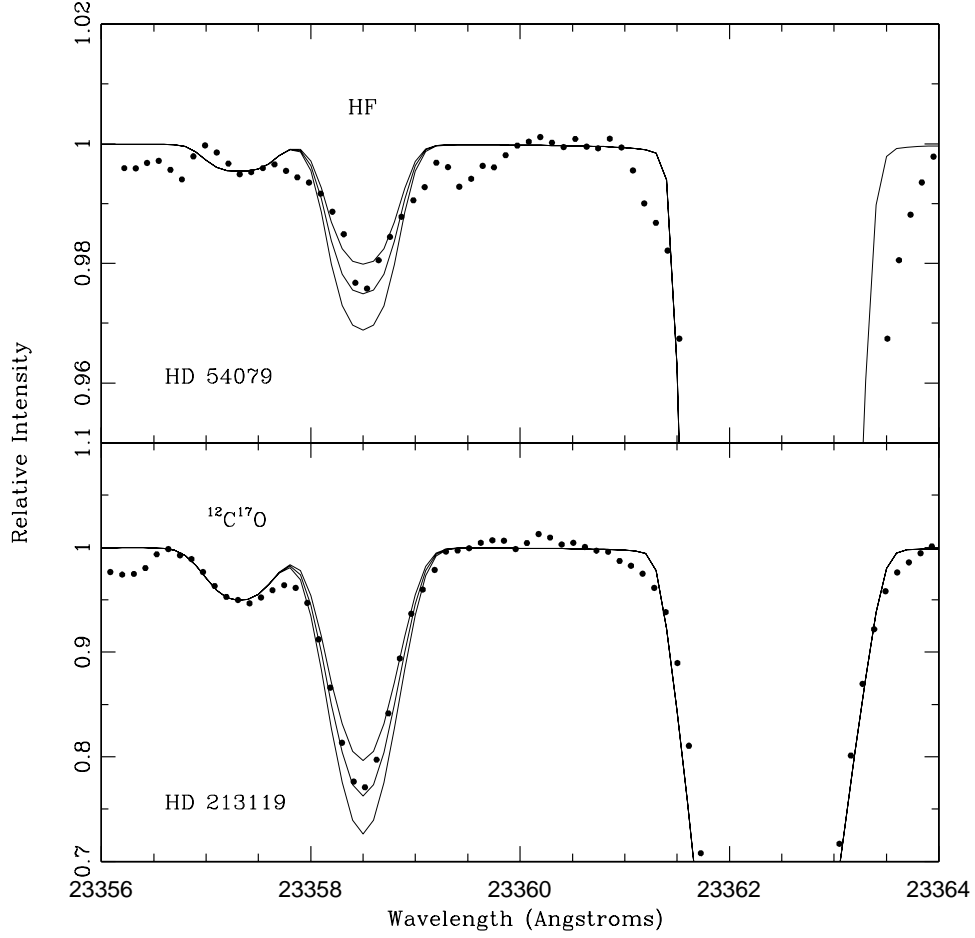


Fig. 1.— HF spectra of two thin disk stars are shown together with calculated synthetic spectra. The upper panel is the spectrum of HD 54079, a giant with a temperature of 4450 K and $[\text{Fe}/\text{H}] = -0.45$. It is shown with synthetic spectra for $\log A(\text{F}) = 3.98, 4.08$, and 4.08 . The lower panel is the spectrum of HD213119, a giant with a temperature of 4090 K and $[\text{Fe}/\text{H}] = -0.50$. It is shown with synthetic spectra for $\log A(\text{F}) = 4.24, 4.34$, and 4.44 . The $^{12}\text{C}/^{17}\text{O}$ feature adjacent to HF has been noted in the lower panel.

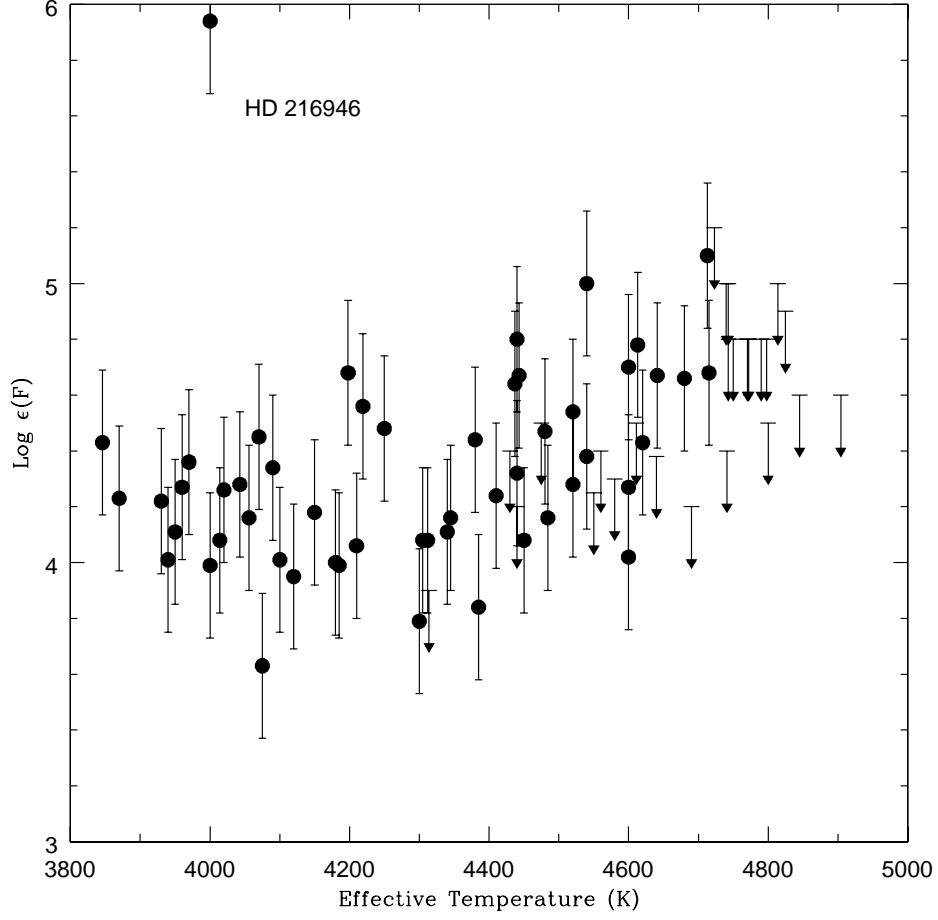


Fig. 2.— Derived abundance of $\log \epsilon(\text{F})$ versus effective temperature. The HF feature becomes undetectable at temperatures above 4700 K. For temperatures $4500 < T_{\text{eff}} < 4700$, HF is detectable only if the abundance is high. The M0Iab supergiant HD 216946 (HR 8726) is labelled.

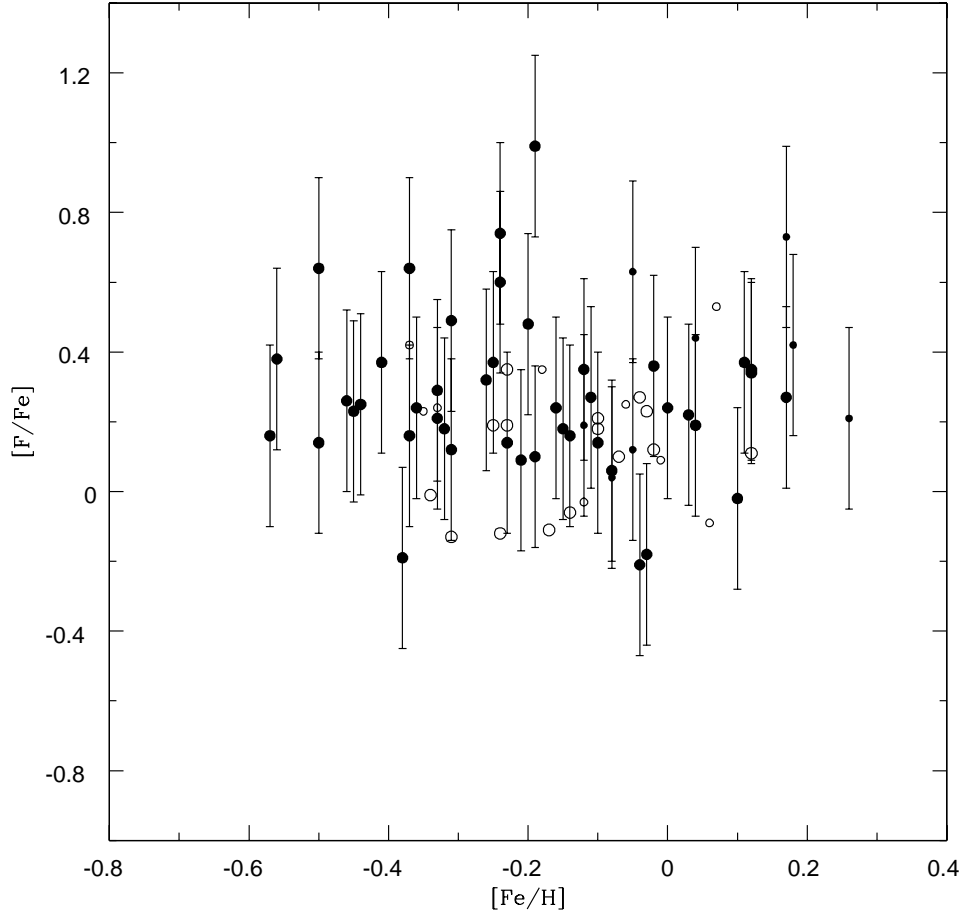


Fig. 3.— Derived abundance of fluorine $[F/Fe]$ versus $[Fe/H]$ plotted together with values from the literature. Stars with temperatures above 4500 K have been omitted, since many are upper limits due to the high temperature. Filled symbols represent stars reported here. Large filled circles are giants and small filled circles are dwarfs from our measurements. Literature measurements from Jorissen et al. (1992), Recio-Blanco et al. (2012), Nault & Pilachowski (2013), and Jönsson et al. (2014b) are shown as open circles.

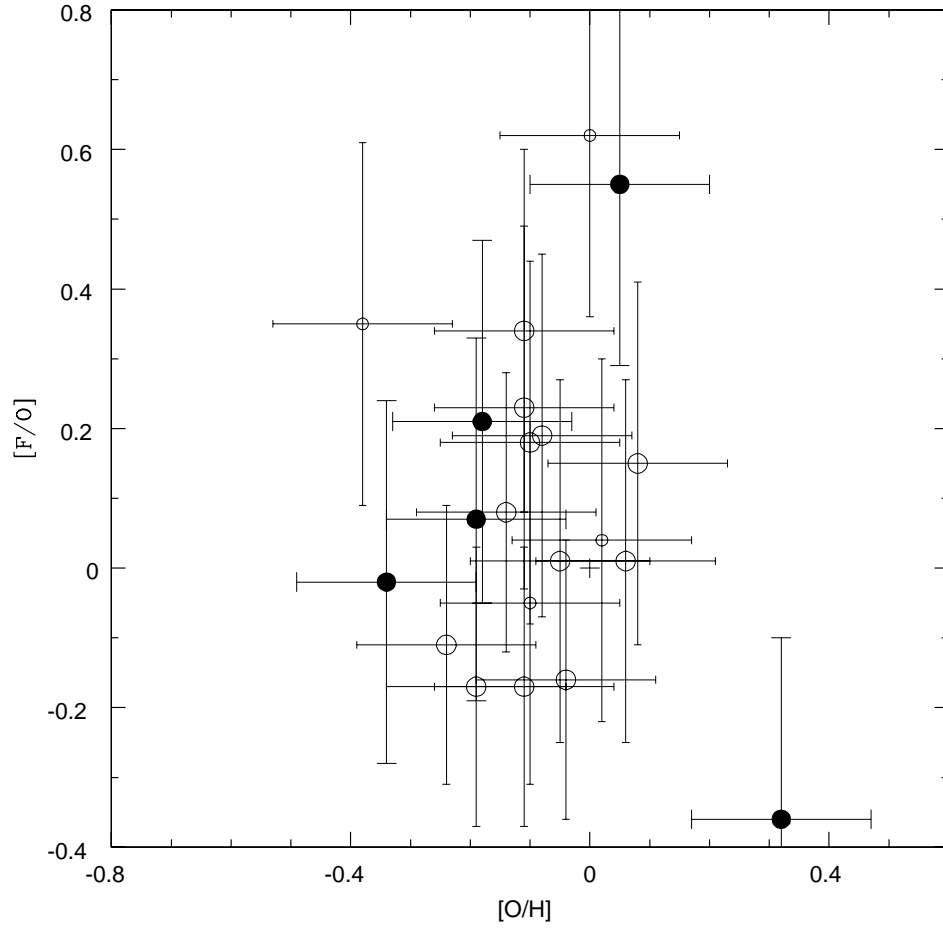


Fig. 4.— $[F/O]$ versus $[O/H]$ for thin disk stars, including measurements from the literature. Symbols are as defined in Fig. 3.

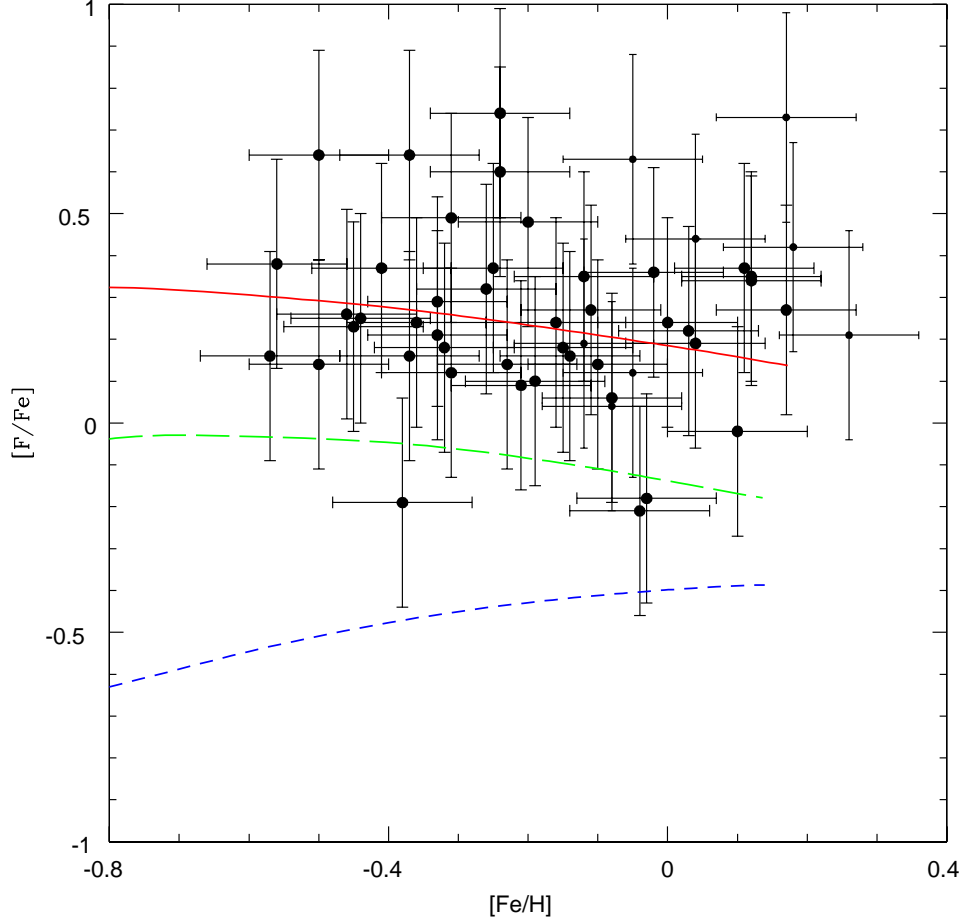


Fig. 5.— $[F/Fe]$ versus $[Fe/H]$ for thin disk stars. Chemical evolution models from Kobayashi et al. (2011) are shown for AGB production (small-dashed blue curve), SN plus AGB production (large-dashed green curve), and SN production with neutrino spallation plus contributions from AGB stars (solid red curve).

Table 1. Stars Observed

HD	HIP	Alt.	Spec. Type	UT Date	K Mag.	Exp. Time (s)	S/N Ratio
6	417	HR 2	G9III:	3 Dec. 2012	3.908	4 x 300	175
5268	4257	21 Cet	G5IV	3 Dec. 2012	3.91	4 x 300	300
5437	4371	22 Cet	K4III	3 Dec. 2012	1.826	4 x 30	200
6805	5364	eta Cet	K1III	5 Dec. 2012	0.875	4 x 30	150
7578	5936	HR 371	K1III	2 Dec. 2012	3.371	4 x 400	130
8207	6411	ksi And	K0III	2 Dec. 2012	2.554	4 x 150	200
9408	7294	chi Cas	G9IIIb	2 Dec. 2012	2.311	4 x 120	180
9900	7617	HR 461	G5Iab:	2 Dec. 2012	2.391	4 x 120	180
9927	7607	ups Per	K3III	2 Dec. 2012	0.649	3 x 30	200
10853	8275	...	K3.5V	4 Dec. 2012	6.319	4 x 900	200
11949	9222	3 Per	K0IV	1 Dec. 2012	3.03	4 x 90	210
12929	9884	alf Ari	K2III	1 Dec. 2012	-0.783	4 x 5	240
13520	10340	b And	K4III	29 Nov. 2012	1.329	4 x 100	250
13789	10416	LTT 1147	K3.5V	1 Dec. 2012	6.015	4 x 900	120
15755	11840	HR 738	K0III	5 Dec. 2012	3.233	4 x 300	192
17660	13258	LHS 1453	K4.5V	4 Dec. 2012	6.128	4 x 900	170
18449	13905	24 Per	K2III	5 Dec. 2012	2.103	4 x 90	190
19270	14439	HR 931	K3III	3 Dec. 2012	3.263	4 x 300	195
20644	15549	HR 999	K4III	1 Dec. 2012	0.877	4 x 20	200
21017	15861	64 Ari	K4III	5 Dec. 2012	2.888	4 x 300	200
26162	19385	...	F8V	3 Dec. 2012	6.944	4 x 300	230
26546	19641	HR 1295	K0III	3 Dec. 2012	3.641	4 x 300	250
27382	20250	phi Tau	K1III	2 Dec. 2012	2.292	4 x 100	280
29139	21421	alf Tau	K5III	2 Dec. 2012	-3.04	4 x 1	200
29697	21818	V834 Tau	K3V	4 Dec. 2012	5.146	4 x 600	150
30454	22393	HR 1529	K1III	3 Dec. 2012	2.482	4 x 100	240
30504	22453	1 Aur	K4III	30 Nov. 2012	1.307	4 x 30	200
30834	22678	2 Aur	K3III	30 Nov. 2012	1.389	4 x 30	240
31539	23043	HR 1585	K1III	30 Nov. 2012	2.669	4 x 100	130
32147	23311	LHS 200	K3V	2 Dec. 2012	3.706	4 x 300	140
33554	24197	HR 1684	K5III	3 Dec. 2012	1.732	4 x 30	280
34043	24450	HR 1709	K4III	3 Dec. 2012	2.537	4 x 100	240
34334	24727	16 Aur	K2.5IIIb	30 Nov. 2012	1.386	4 x 30	170
35620	25541	phi Aur	K3IIICN	3 Dec. 2012	2.104	4 x 90	200
36003	25623	LHS 1763	K5V	4 Dec. 2012	4.88	4 x 600	150
37984	26885	b Ori	K1III	2 Dec. 2012	2.212	4 x 100	290
39019	27581	135 Tau	G9III:	3 Dec. 2012	3.383	4 x 300	300
39118	27588	HR 2024	G8III	29 Nov. 2012	3.337	4 x300	350
39715	27918	LHS 1798	K3V	3 Dec. 2012	6.352	4 x 900	170
40657	28413	HR 2113	K1.5III	30 Nov. 2012	1.649	4 x 60	150
43039	29696	kap Aur	G8.5IIIb	5 Dec. 2012	1.712	6 x 200	300
47174	31832	50 Aur	K3Iab:	5 Dec. 2012	1.931	4 x 200	100
47752	32010	G 109-20	K3.5V	4 Dec. 2012	5.546	4 x 900	300
49293	32578	18 Mon	K0IIa	5 Dec. 2012	1.849	5 x 200	120
52556	33914	HR 2632	K1III:	1 Dec. 2012	3.105	4 x 300	100

Table 1—Continued

HD	HIP	Alt.	Spec. Type	UT Date	K Mag.	Exp. Time (s)	S/N Ratio
52960	34033	HR 2649	K3III	1 Dec. 2012	2.044	4 x 120	100
54079	34387	HR 2682	K0III:	29 Nov. 2012	3.036	4 x 200	200
54716	34752	63 Aur	K3.5III	1 Dec. 2012	1.605	4 x 45	290
54719	34693	tau Gem	K2III	1 Dec. 2012	1.681	4 x 45	150
58207	36046	iot Gem	G9IIIb	5 Dec. 2012	1.562	4 x 100	170
58972	36284	gam CMi	K3III	1 Dec.2012	0.993	4 x 30	230
60522	36962	ups Gem	M0III	30 Nov. 2012	0.232	4 x 10	175
63752	38253	HR 3047	K3III	30 Nov. 2012	2.414	4 x 100	200
65277	38931	G 113-7	K3V	4 Dec. 2012	5.511	4 x 900	200
65953	39211	V645 Mon	K4III	30 Nov. 2012	1.164	4 x 30	200
66141	39311	HR 3145	K2III	30 Nov. 2012	1.447	4 x 30	250
87883	49699	...	K0V	3 Dec. 2012	5.314	4 x 600	200
88320	F2III	3 Dec. 2012	9.038	4 x 300	200
209747	109068	22 Peg	K4III	3 Dec. 2012	1.672	4 x 30	150
209945	109102	HR 8424	K5III	3 Dec. 2012	1.295	20 x 30	200
210354	109354	27 Peg	G6III:	3 Dec. 2012	3.169	4 x 90	130
210762	109602	HR 8466	K0	3 Dec. 2012	2.567	4 x90	190
211075	109793	...	K2	1 Dec. 2012	5.217	4 x 400	170
213119	110986	36 Peg	K5III	1 Dec. 2012	1.882	4 x 30	210
214868	111944	11 Lac	K2III	4 Dec. 2012	1.668	4 x 60	200
214995	112067	...	K2 III	4 Dec. 2012	6.339	4 x 300	180
215182	112158	eta Peg	G2II-III	5 Dec. 2012	1.018	7 x 15	200
215665	112440	lam Peg	G8Iab:	4 Dec. 2012	1.508	4 x 60	250
216174	112731	HR 8688	K1III	1 Dec. 2012	2.625	4 x 60	200
216646	113084	HR 8712	K0III	4 Dec. 2012	3.514	4 x 300	250
216946	113288	V424 Lac	M0Iab:	5 Dec. 2012	0.724	4 x 60	180
218031	113919	LTT 16772	K0IIIb	5 Dec. 2012	2.154	4 x 300	100
219134	114622	HR 8832	K3V	4 Dec. 2012	3.26	4 x 300	300
220009	115227	7 Psc	K2III	2 Dec. 2012	1.993	4 x 90	280
222107	116584	lam And	G8III	5 Dec. 2012	1.466	4 x 80	300
223559	117567	HR 9029	K4III	3 Dec. 2012	2.058	4 x 90	100
223807	117756	HR 9040	K0III	5 Dec. 2012	3.186	4 x 300	100
225212	355	3 Cet	K3Iab:	3 Dec. 2012	1.398	4 x 60	250
233517	K2	30 Nov. 2012	6.637	4 x 900	200

Table 2. Stellar Parameters and Fluorine Abundances

Star	T_{eff} (K)	Log g	ξ (km s $^{-1}$)	[Fe/H]	Ref	F EQW (mÅ)	Log $\epsilon(F)$
HD 6	4580	2.70	2.1	0.01	a	<10	<4.3
HD 5268	4904	2.35	2.0	−0.57	b	<9	<4.6
HD 5437	3940	1.67	2.1	−0.31	a	140	4.01
HD 6805	4520	2.80	2.1	−0.03	a	15.8	4.28
HD 7578	4680	2.50	1.4	0.12	c	10.5	4.66
HD 8207	4750	2.75	1.5	0.27	c	<20	<4.8
HD 9408	4814	2.46	2.0	−0.31	b	<19	<4.5
HD 9900	4430	1.18	3.5	−0.05	d	<25	<4.4
HD 9927	4380	2.34	2.3	0.00	a	37.7	4.44
HD 10853	4600	4.65	0.8	−0.12	c	10.5	4.27
HD 11949	4845	2.85	1.2	−0.09	e	<10	<4.6
HD 12929	4600	2.70	1.7	−0.13	f	29.9	4.7
HD 13520	4043	1.66	2.1	−0.16	b	157	4.28
HD 13789	4740	4.33	0.8	−0.06	g	<30	<5.0
HD 15755	4611	2.30	1.2	−0.01	c	<11	<4.5
HD 17660	4713	4.75	0.8	0.17	c	31	5.1
HD 18449	4340	2.37	2.0	−0.19	a	34	4.11
HD 19270	4723	2.40	1.5	0.15	c	<22	<5.2
HD 20644	4100	1.65	3.0	−0.44	f	93	4.01
HD 21017	4443	2.74	1.9	0.12	b	40.9	4.67
HD 26162	4640	2.87	2.2	−0.02	a	<9	<4.4
HD 26546	4743	2.25	1.3	−0.01	c	<20	<5.0
HD 27382	4480	2.67	2.0	−0.37	a	40	4.47
HD 29139	3870	1.66	2.1	−0.04	b	192	4.23
HD 29697	4440	4.19	0.5	0.18	h	68	4.8
HD 30454	4540	2.60	1.9	−0.31	a	23.6	4.38
HD 30504	4056	1.79	2.1	−0.33	b	136	4.16
HD 30834	4219	1.59	2.3	−0.24	b	134	4.56
HD 31539	4210	2.21	2.1	−0.32	a	57.7	4.06
HD 32147	4641	4.60	1.1	0.26	i	16.8	4.67
HD 33554	3970	1.71	2.0	−0.11	a	197	4.36
HD 34043	4120	2.00	2.2	−0.04	a	48.1	3.95
HD 34334	4180	2.12	1.9	−0.46	a	80	4.0
HD 35620	4198	1.92	2.4	0.15	b	98.7	4.68
HD 36003	4345	4.59	0.5	−0.15	b	16.5	4.16
HD 37984	4484	2.21	2.0	−0.41	b	19.8	4.16
HD 39019	4770	2.82	2.1	−0.08	a	<14	<4.8
HD 39118	4550	1.52	2.2	−0.10	f	<9	<4.25
HD 39715	4798	4.75	0.9	−0.04	j	<16	<4.8
HD 40657	4300	1.83	2.3	−0.57	b	29.1	3.79
HD 43039	4690	2.81	2.0	−0.33	a	<5	<4.2
HD 47174	4410	2.30	2.2	−0.10	a	30	4.24
HD 47752	4613	4.60	0.8	−0.05	c	30.2	4.78
HD 49293	4620	2.59	2.3	−0.12	a	<12	<4.4
HD 52556	4700	2.65	2.3	−0.08	f	<18	...

Table 2—Continued

Star	T_{eff} (K)	Log g	ξ (km s ⁻¹)	[Fe/H]	Ref	F EQW (mÅ)	Log $\epsilon(F)$
HD 52960	4150	1.80	2.0	-0.08	f	64.2	4.18
HD 54079	4450	2.10	1.8	-0.45	f	14.1	4.08
HD 54716	4020	1.88	2.2	-0.26	a	150	4.26
HD 54719	4437	2.17	2.0	0.17	b	32	4.64
HD 58207	4825	2.57	2.1	-0.11	b	<12	<4.9
HD 58972	4000	1.82	2.2	-0.37	a	116	3.99
HD 60522	3846	1.69	2.5	0.04	b	250	4.43
HD 63752	4075	1.00	2.4	-0.38	f	48.8	3.63
HD 65277	4741	4.76	0.8	-0.16	j	<3	<4.4
HD 65953	4014	1.81	2.2	-0.21	b	128	4.08
HD 66141	4312	2.11	1.9	-0.36	b	39.3	4.08
HD 87883	4772	4.44	0.8	0.09	k	<15	<4.8
HD 88320	3960	4.45	0.8	-0.05	b	37.8	4.27
HD 209747	4070	1.84	2.2	0.02	a	149	4.45
HD 209945	3930	1.62	2.5	-0.14	a	188	4.22
HD 210354	4790	2.81	1.9	-0.24	a	<15	<4.8
HD 210762	4185	1.65	2.5	-0.03	f	37.5	3.99
HD 211075	4305	1.76	1.8	-0.33	l	39.4	4.08
HD 213119	4090	1.65	2.5	-0.50	f	188	4.34
HD 214868	4440	2.32	2.4	-0.25	a	26.7	4.32
HD 214995	4560	2.67	2.2	-0.09	a	<9	<4.4
HD 215182	5080	2.48	2.3	-0.22	a	<5	<5.0
HD 215665	4800	3.30	3.0	-0.10	a	<6	<4.5
HD 216174	4385	1.87	2.0	-0.50	b	17	3.84
HD 216646	4520	2.63	2.3	-0.02	a	24.2	4.54
HD 216946	4000	0.50	2.4	-0.07	m	225	5.94
HD 218031	4743	2.46	2.0	-0.16	b	<15	<4.8
HD 219134	4715	4.57	0.7	0.06	b	22	4.68
HD 220009	4314	1.81	2.1	-0.71	b	<35.9	<3.9
HD 222107	4600	3.11	2.0	-0.56	a	10	4.02
HD 223559	3950	1.67	2.2	-0.23	a	152	4.11
HD 223807	4440	2.56	2.2	-0.10	a	<12	<4.2
HD 225212	4250	0.75	4.5	-0.20	h	118	4.48
HDE 233517	4475	2.25	1.9	-0.37	n	<35	<4.5

References. — (a) McWilliam 1990; (b) Prugniel et al. 2011; (c) Mishenina et al. 2006, 2008; (d) Lyubimkov 2010; (e) Takeda et al. 2008 (f) Hekker et al. 2007; (g) Sousa et al. 2008 (h) Luck & Bond 1980, Luck & Heiter 2006; (i) Allende Prieto et al. 2004; (j) Valenti & Fischer 2005; (k) Kotoneva 2006; (l) Melendez et al. 2008; (m) Ramírez et al. 2000; (n) Balachandran et al. 2000.

Table 3. Sensitivity to Stellar Parameters

Parameter	$\log \epsilon(F)$	$\log \epsilon(F)$
	Dwarfs	Giants
$\Delta T_{eff} = +100$ K	+0.18	+0.25
$\Delta \text{Log } g = +0.3$	0.00	–0.02
$\Delta \xi = +0.5$ km s ^{–1}	0.00	–0.01
$\Delta [\text{Fe}/\text{H}] = +0.1$	+0.05	+0.05